Crystal structure, microstructure, surface morphology, and transport properties of $Er_5Ba_7Cu_{12}O_y$ high-temperature-superconductor thin films

K. M. Choudhary, P. Seshadri, J. Bae, and M. Black
Department of Electrical Engineering, Materials Science and Engineering Program, University of Notre Dame, Notre Dame, Indiana 46556

A. Lewicki
Department of Physics, Purdue University, West Lafayette, Indiana 47907

(Received 22 April 1993)

$Er_5Ba_7Cu_{12}O_y$ is a thin-film high-temperature superconductor (critical transition temperature, $T_c=93$ K). The crystal structure, microstructure, surface morphology, and transport properties of $Er_5Ba_7Cu_{12}O_y$ thin films were investigated by x-ray diffraction (XRD), scanning electron microscopy (SEM), and four-point dc-resistivity measurements under magnetic fields. Oriented $Er_5Ba_7Cu_{12}O_y$ thin films on cubic $ZrO_2(100)$, MgO(100), $LaAlO_3(100)$, and $SrTiO_3(100)$ substrates were prepared by molecular-beam deposition and post annealing in wet and dry O_2 (BaF_2 technique; annealing temperature $=850-890$ °C). The 0.4-μm $Er_5Ba_7Cu_{12}O_y$ thin films on cubic $ZrO_2(100)$ and MgO(100) substrates grew with mixed b and c orientations. The 0.4-μm $Er_5Ba_7Cu_{12}O_y$ thin films on $LaAlO_3(100)$ and $SrTiO_3(100)$ substrates annealed at 850 °C had c- and a-oriented grains, whereas the films annealed in the temperature range 870–890 °C displayed (001) epitaxy. By XRD, the lattice constants of $Er_5Ba_7Cu_{12}O_y$ were derived as $a_0=10.38$ Å, $b_0=10.52$ Å, $c_0=11.65$ Å, and $\alpha=\beta=\gamma=90°$. In the SEM studies, the 0.4-μm $Er_5Ba_7Cu_{12}O_y$ thin films were found to have a smooth-surface morphology. The shape of a-oriented grains in the $Er_5Ba_7Cu_{12}O_y$ thin films was found to be thick-rod-like. The transport data of superconducting resistive transitions under magnetic fields (0–5 T) were analyzed with the models of thermally activated giant flux creep. The activation energy for flux creep was determined to be U (K) $=[3\times10^4(1-T/T_c)^{1.8}]/H^{0.7}$ ($H_\perp ab$ plane), where H = magnetic field (T) and T = temperature (K).

I. INTRODUCTION

The structure and properties of high-temperature-superconductor materials are important areas of solid-state research.[1–4] In the R-Ba-Cu-O system (R = Y, Nd, Sm, Eu, Gd, Dy, Ho, or Er), $RBa_2Cu_3O_{7-\delta}$ is one of the most interesting high-temperature-superconductor materials (critical transition temperature, $T_c=92$ K). Studies of compositional variations in the R-Ba-Cu-O system have led to the discovery of other high-T_c superconductors such as $RBa_2Cu_4O_8$ and $R_2Ba_4Cu_7O_{14}$.[3] $R_{1+x}Ba_{2-x}Cu_3O_y$ ($R\neq$Y or Er) oxides also have a $RBa_2Cu_3O_{7-\delta}$-type crystal structure in which the excess R atoms substitutionally occupy the Ba sites.[4–6] In case of R = Y or Er, which are much smaller atoms than Ba, it has been suggested that the $R_{1-x}Ba_{2-x}Cu_3O_y$ structure is not stable and the material decomposes into multiple phases ($Er_1Ba_2Cu_3O_{7-\delta}$, Er_2BaCuO_5, and CuO).[2] Recently, we reported on the discovery of single-phase $Er_5Ba_7Cu_{12}O_y$ high-T_c superconductor thin films ($T_c=93$ K).[7,8] The $Er_5Ba_7Cu_{12}O_y$ thin films have been characterized by x-ray diffraction (XRD),[8] scanning electron microscopy (SEM), and four-point dc resistivity measurements under magnetic fields. The results are reviewed in this paper.

The crystal structure of the $Er_5Ba_7Cu_{12}O_y$ thin films was investigated by XRD. Oriented $Er_5Ba_7Cu_{12}O_y$ thin films of various thicknesses were grown on $LaAlO_3(100)$, $SrTiO_3(100)$, MgO(100), and cubic $ZrO_2(100)$ substrates by molecular-beam deposition of Er, BaF_2, and Cu (oxygen pressure $=5\times10^{-6}$ torr) followed by post annealing in wet and dry O_2 (annealing temperature $=850-890$ °C). The composition of some of the films was checked by Rutherford backscattering spectroscopy (RBS).[9] Using the XRD data, the lattice parameters of the unit cell of $Er_5Ba_7Cu_{12}O_y$ were determined as shown in this paper.

The SEM studies provided information on the surface morphology of the $Er_5Ba_7Cu_{12}O_y$ thin films. These studies also substantiated that the oriented $Er_5Ba_7Cu_{12}O_y$ thin film is a single-phase material. The $Er_1Ba_2Cu_3O_{7-\delta}$ and $Er_5Ba_7Cu_{12}O_y$ thin films on $LaAlO_3(100)$ and $SrTiO_3(100)$ substrates were examined (film thickness 0.2–0.4 μm). For the $RBa_2Cu_3O_{7-\delta}$ thin films on $LaAlO_3(100)$ and $SrTiO_3(100)$ substrates, which are grown by the BaF_2 technique (850–890 °C post anneal), it has been reported that the 0.2-μm thin films are mostly c oriented [(001) epitaxy], but the growth mode changes to (100) epitaxy when the thickness is greater than 0.2 μm.[10] These results were obtained by high-resolution electron microscopy and transmission electron microscopy by several groups.[10,11] The a-oriented grains of $RBa_2Cu_3O_{7-\delta}$ thin films are needle-like in shape.[10–13] As a result, the $RBa_2Cu_3O_{7-\delta}/LaAlO_3(100)$ thin films with thicknesses ≥0.2 μm have both c- and a-oriented growth modes, in which the a-oriented grains are in a netlike pattern near the surface whereas the c-oriented

0163-1829/93/48(13)/9697(13)/$06.00

grains are buried.[10,11] Our $ErBa_2Cu_3O_{7-\delta}/LaAlO_3(100)$ thin films show a similar surface morphology. On the other hand, the SEM results for the $Er_5Ba_7Cu_{12}O_y/LaAlO_3(100)$ thin films show that the (001) epitaxy continues in thicker layers (>0.2 μm) for the same post-annealing temperature. Furthermore, the *a*-oriented grains of $Er_5Ba_7Cu_{12}O_y$ are thicker in cross section in the *ab* plane than the *a*-oriented grains of $ErBa_2Cu_3O_{7-\delta}$.

The four points dc-resistivity measurements under magnetic fields were used to study thermally activated flux creep below T_c in the $Er_5Ba_7Cu_{12}O_y$ thin films. The resistivity (ρ) versus temperature [T (K)] data were fitted to the models of flux creep.[14–16] In type-II superconductors in the vortex state under magnetic fields, magnetic flux bundles penetrate the sample, which are also surrounded by supercurrent loops. According to the conventional flux-creep model of Anderson and Kim for the type-II superconductors in the vortex state, there is always a finite small resistance below T_c which is due to thermally activated motion of the vortex lines.[14] The creep velocity is given by the formula[17]

$$v_\phi=(\nu_0 x)\exp(-U/k_BT)\sinh(W/k_BT)\ , \tag{1}$$

where ν_0 is the attempt frequency for flux hopping, x is the average hopping distance, U is the activation energy for flux motion, $W(J,H)$ is the energy due to the Lorentz force acting on a macroscopic current J, which is induced by the flux motion, T is the temperature (K); and k_B is the Boltzmann constant. The electric-field gradient due to the thermally activated flux motion gives a finite resistivity ρ_{sc} to the macroscopic current J, which is given by the equation

$$\rho_{sc}=(v_\phi H)/J \tag{2a}$$

or

$$\rho_{sc}=(\nu_0 xH/J)\exp(-U/k_BT)\sinh(W/k_BT)\ . \tag{2b}$$

Below T_c, the measured conductivity σ_{eff} is a sum of σ_{sc} and normal-state conductivity from a volume fraction which is not superconducting.[18] When the normal-state conductivity approaches zero, $\sigma_{eff}=\sigma_{sc}$, or $\rho_{eff}=\rho_{sc}$. If the applied current density is the four-point dc-resistivity measurements is much smaller than the depinning critical current density, J_c, then the term W/k_BT will be small. In that case,

$$\rho_{sc}=[\nu_0 xHW/(Jk_BT)]\exp(-U/k_BT) \tag{3a}$$

or

$$\rho_{sc}/H=A\exp(-U/k_BT)\ , \tag{3b}$$

where $A=\nu_0 xW/(Jk_BT)$, which can be treated as a constant for constant J and H if the temperature range is not large. In the Anderson-Kim model of flux creep, if the temperature dependence of U is neglected then the magnetic-field dependence of U can be described by the expression[19]

$$U=U_0H^{-\gamma}\ , \tag{4}$$

where γ is the exponent.

For the $RBa_2Cu_3O_{7-\delta}$ high-T_c superconductors, a modified (giant) flux-creep model has been found to work well.[15–17] The giant flux-creep model takes the temperature dependence and magnetic-field dependence of activation energy into account. In this model,

$$U=[U_0(1-t)^\alpha]/H^\beta\ , \tag{5}$$

where U_0 is a constant for a high-T_c material (activation energy constant), $t=T/T_c$, and exponents α,β are constants. In theory $\alpha=1.5$ and $\beta=1$.[15,16] Experimentally, Zhu *et al.* have found the values of α and β to be 1.8 and 1 for epitaxial $YBa_2Cu_3O_{7-\delta}(001)$ thin films.[17]

In our experiments, the objective of the transport studies under magnetic fields was to compare the flux-creep behavior of $Er_5Ba_7Cu_{12}O_y$ and $ErBa_2Cu_3O_{7-\delta}$ high-T_c superconductor thin films. Recently, it has been reported that in the case of pure $YBa_2Cu_3O_{7-\delta}$ single crystals there is a vortex glass transition ($T_g=74$ K) in magnetic fields ≥ 7 T.[20] In the vortex glass model of high-T_c superconductors, the resistance truly goes to zero below the glass transition temperature, T_g, in a second-order phase transition.[20,21] We did not make attempt to search for the vortex glass transition. The modified flux-creep model was found to be sufficient to describe the transport data for the $Er_5Ba_7Cu_{12}O_y(001)$ thin films.

II. EXPERIMENTAL DETAILS

The $Er_5Ba_7Cu_{12}O_y$ and $ErBa_2Cu_3O_{7-\delta}$ thin films were prepared by molecular-beam deposition (MBD) and post annealing using the BaF_2 technique. The ultrahigh vacuum (UHV) MDB system consists of effusion cells, an oxygen nozzle with a slow leak valve, a movable (water-cooled) thin-film thickness monitor (FTM), a residual gas analyzer, and a sample transfer assembly. The effusion cells of Er, BaF_2, and Cu have alumina crucibles ($\frac{3}{8}$-in. orifice diameter 3 in. long) with inserts of Ta foils. Each effusion cell has a W5%Re-W26%Re thermocouple inserted in an alumina slug. The thermocouple touches the bottom of the crucible. The effusion cells are wrapped with several layers of Ta foils for radiation shielding to prevent excessive outgassing.

The Er, BaF_2, and Cu vapors in stoichiometric ratio were deposited on $LaAlO_3(100)$, $SrTiO_3(100)$, cubic $ZrO_2(100)$, and MgO(100) substrates at room temperatures (RT) in the presence of 5×10^{-6} torr O_2. Usually, the base was about 2×10^{-10} torr, whereas the pressure just before leaking in O_2 was in the 1×10^{-8}–3×10^{-8} torr range. The flux (arrival rate) of each kind of vapor at the substrate was determined by moving the quartz crystal FTM at the position of the substrate and measuring the deposition rate in Å/sec before deposition. For accurate measurements with the FTM, the film was deposited for 30 sec or more and then the readout of total thickness was divided by time to get the deposition rate. Note that the flux is calculated from the deposition rate. After deposition, the mixture films were taken out from the UHV system and post annealed in wet and dry O_2 at a temperature in the 850–890 °C range to get the epitaxi-

al (or oriented) $Er_5Ba_7Cu_{12}O_y$ or $ErBa_2Cu_3O_{7-\delta}$ single-phase thin films. The film thickness after post annealing was in the 0.2–1.2 μm range, but most of the films were either 0.2 or 0.4 μm thick. The composition of some of the films was verified by Rutherford backscattering spectroscopy, as mentioned earlier.[9] The $Er_5Ba_7Cu_{12}O_y$ and $ErBa_2Cu_3O_{7-\delta}$ thin films were characterized by x-ray diffraction, scanning electron microscopy, and measurements of transport properties under magnetic fields as described below.

The XRD patterns of the $Er_5Ba_7Cu_{12}O_y$ thin films were obtained with a DIANO diffractometer using a Cu K_α source ($\lambda=1.542$ Å). The diffraction intensity (counts) versus Bragg angle, 2θ, data were acquired in the 5°–85° range. The scan rate was 0.2°.

The surface morphology and microstructure of the $Er_5Ba_7Cu_{12}O_y$ and $ErBa_2Cu_3O_{7-\delta}$ thin films were studied with an ISI Model 60A scanning electron microscope. The microscope was mostly operated in the backscattering mode, although the secondary electron detection mode of SEM was also applied.[22] Note that in the backscattering mode of SEM operation the Z contrast of phases is enhanced (Z is the atomic number). Hence, the backscattering mode is very useful for the identification of second-phase grains. The SEM pictures were taken at magnifications in the 500–10 K range.

The transport properties of the epitaxial $Er_5Ba_7Cu_{12}O_y(001)/LaAlO_3(100)$ thin films were investigated by four-point dc-resistivity measurements. For the resistivity measurements, the samples were cut in the size 2.5 mm×6 mm, approximately. Four collinear silver pads were deposited along the length of each sample by thin film vapor deposition (Ag film thickness=0.5 μm). The electrical leads were connected to the silver pads by soldering with pure indium. In each measurement, a sample holder mounted with one sample was placed in a cryogenic measurement system (LAKE SHORE Model DRC-91C controller, CRYOGENIC Model SCU 500 cryostat, and HP Model 34401 voltmeter). The resistivity measurements were done in applied magnetic fields of 0–5 T. The magnetic field was applied perpendicular to the ab plane of the epitaxial $Er_5Ba_7Cu_{12}O_y/LaAlO_3(100)$ thin films. Note that the single-phase $Er_5Ba_7Cu_{12}O_y$ material has an orthorhombic crystal structure for which the lattice parameters a_0 and b_0 are much different from the lattice constants a_0' and b_0' of $ErBa_2Cu_3O_{7-\delta}$, as shown in Sec. III. A constant current of 0.1 or 1.0 mA was applied between the outer two silver pads and the voltage drop between the central two pads was measured (measured resistance=voltage drop divided by constant current). The measured resistance values were converted into resistivity.

III. DATA ANALYSIS AND RESULTS

A. X-ray diffraction

Figures 1(a) and 1(b) show the XRD patterns for 0.4-μm $Er_5Ba_7Cu_{12}O_y$ thin films on $LaAlO_3(100)$ and $SrTiO_3(100)$ substrates. The films were annealed at 850 °C. The interplanar spacings, d_{hkl}, were calculated according to Bragg's law. In the calculations, corrections for sample displacement error were also made.[5,8,23] The results are shown in a tabulated form in Ref. 8. The diffraction patterns indicate that the film is primarily c oriented. Using the experimental d_{001} values, the lattice parameter c_0 of $Er_5Ba_7Cu_{12}O_y$ was determined to be 11.65±0.02 Å, which has been reported earlier. In Figs. 1(a) and 1(b), another mode of oriented growth is also observed for which the diffraction peaks are labeled as $h00$. At this point, it has been hypothesized that the $Er_5Ba_7Cu_{12}O_y$ material has an orthorhombic crystal structure. A justification for this hypothesis is given later. Using the interplanar spacings, d_{h00}, for the first-order and higher-order diffraction peaks, the lattice constant a_0 is derived as 10.38±0.02 Å.

In Fig. 2(a), the XRD pattern for a 1.2-μm $Er_5Ba_7Cu_{12}O_y$ thin film on a cubic $ZrO_2(100)$ substrate is shown, whereas Fig. 2(b) shows the XRD spectrum of a 0.5-μm $Er_5Ba_7Cu_{12}O_y$ thin film on a MgO(100) substrate. These films were post annealed at 880 °C. The diffraction patterns show a dominant b-oriented growth of $Er_5Ba_7Cu_{12}O_y$ thin films. The lattice constant b_0 is determined to be 10.52±0.02 Å. The $0k0$ and $00l$ diffraction

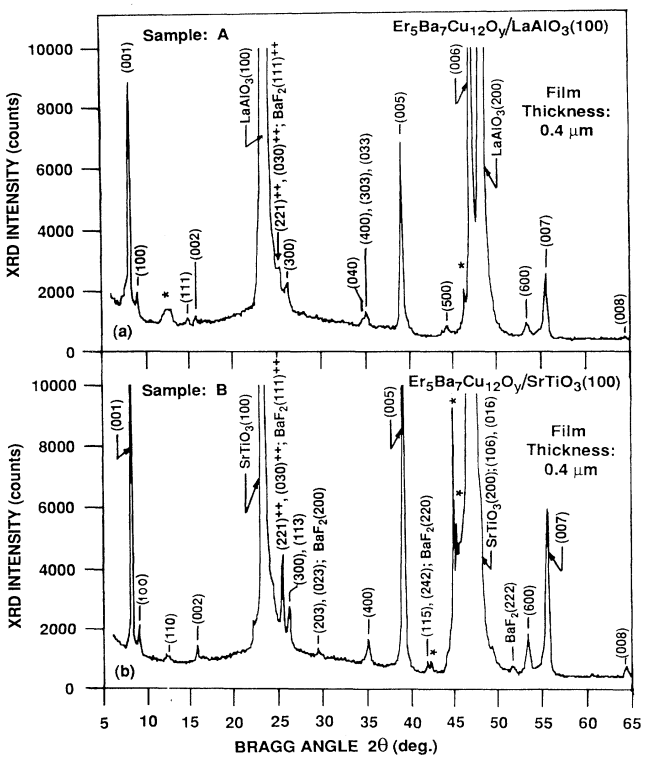

FIG. 1. XRD patterns for 0.4-μm $Er_5Ba_7Cu_{12}O_y$ thin films on $LaAlO_3(100)$ and $SrTiO_3(100)$ substrates (x-ray source, Cu K_α; $\lambda=1.542$ Å). The diffraction peaks were indexed with the lattice parameters of $Er_5Ba_7Cu_{12}O_y$ as described in the text ($a_0=10.38$ Å, $b_0=10.52$ Å, $c_0=11.65$ Å, and $\alpha=\beta=\gamma=90°$). (a) Diffraction intensity (counts) versus Bragg angle, 2θ (deg) for $Er_5Ba_7Cu_{12}O_y/LaAlO_3(100)$. (b) Diffraction intensity (counts) versus Bragg angle, 2θ (deg) for $Er_5Ba_7Cu_{12}O_y/SrTiO_3(100)$. [(*) Peak due to diffraction from the substrate or K_β x rays; (++) Bragg angle could not be measured accurately].

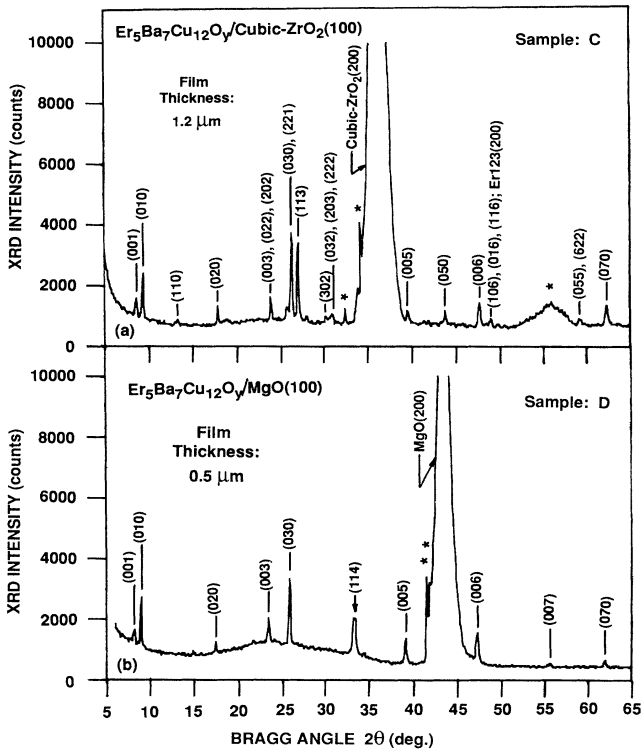

FIG. 2. XRD patterns for $Er_5Ba_7Cu_{12}O_y$ thin films on cubic $ZrO_2(100)$ and MgO(100) substrates (x-ray source, Cu K_α; $\lambda = 1.542$ Å). The diffraction peaks were indexed with the lattice parameters of $Er_5Ba_7Cu_{12}O_y$ as described in the text. (a) Diffraction intensity (counts) versus Bragg angle, 2θ (deg) for 1.2-μm $Er_5Ba_7Cu_{12}O_y$/cubic $ZrO_2(100)$. (b) Diffraction intensity (counts) versus Bragg angle, 2θ (deg) for 0.5-μm $Er_5Ba_7Cu_{12}O_y$/MgO(100). [(*) Peak due to diffraction from the substrate or K_β x rays].

peaks are indexed in the figures. The 0.5-μm $Er_5Ba_7Cu_{12}O_y$ thin film on the MgO(100) substrate has *b*- and *c*-oriented growths only [Fig. 2(a)]. Although the 1.2-μm $Er_5Ba_7Cu_{12}O_y$ thin film on the cubic $ZrO_2(100)$ substrate has *b*- and *c*-oriented growths, it also has a large volume of polycrystalline material. Consequently, the XRD pattern for 1.2-μm $Er_5Ba_7Cu_{12}O_y$ on cubic $ZrO_2(100)$ shows some high-index diffraction peaks such as 113 and 116. A comparison between the experimentally derived d_{hkl} values and $d_{hkl(\text{model})}$ has been shown in Ref. 8. The agreement between $d_{hkl(\text{expt})}$ and $d_{dhl(\text{model})}$ is excellent. Therefore, the unit cell of $Er_5Ba_7Cu_{12}O_y$ is understood. The lattice parameters of $Er_5Ba_7Cu_{12}O_y$ are derived as $a_0 = 10.38 \pm 0.02$ Å, $b_0 = 10.52 \pm 0.02$ Å, and $c_0 = 11.65 \pm 0.02$ Å and the crystallographic angles are $\alpha = \beta = \gamma = 90°$.

We would like to comment on the superconducting resistive transitions and metallicity of the $Er_5Ba_7Cu_{12}O_y$ thin films on $LaAlO_3(100)$, $SrTiO_3(100)$, cubic $ZrO_2(100)$, and MgO(100) substrates. The $Er_5Ba_7Cu_{12}O_y$ thin films on $LaAlO_3(100)$ and $SrTiO_3(100)$ substrates show metallic behavior and sharp resistive transitions ($T_c = 93$ K).[7,8] The *b*-oriented $Er_5Ba_7Cu_{12}O_y$ thin films on the cubic $ZrO_2(100)$ substrate show semiconducting behavior but the onset of superconducting transition is at 92 K and the transition is broad. The *b*-oriented $Er_5Ba_7Cu_{12}O_y$ thin films on the MgO(100) substrate show $T_{c,\text{onset}}$ at about 83 K.

B. Scanning electron microscopy

The SEM pictures of a 0.2-μm $Er_5Ba_7Cu_{12}O_y$ thin film on the $LaAlO_3(100)$ substrate, which was post annealed at 890 °C, are depicted in Figs. 3(a) and 3(b). The SEM picture shown in Fig. 3(a) was taken at 3 K magnification whereas the picture shown in Fig. 3(b) was taken at a magnification of 10 K. The film shows (001) epitaxy, which was also confirmed by x-ray diffraction. The surface is smooth. The pictures show few rods of *a*- or *b*-oriented growth in the surface region. From the *Z* contrast of second phases (*z* is the atomic number), any significant amount of second phases was not observed. If the $Er_5Ba_7Cu_{12}O_y$ thin film is not a single-phase material, then it will decompose into three phases according to the formula

$$Er_5Ba_7Cu_{12}O_y = \underset{(74\text{ vol. \%})}{3Er_1Ba_2Cu_3O_{7-\delta}} + \underset{(18\text{ vol. \%})}{Er_2BaCuO_5} + \underset{(6\text{ vol. \%})}{2CuO}\ . \tag{6}$$

Since the phase decomposition is not observed, the SEM results substantiate that the $Er_5Ba_7Cu_{12}O_y$ thin film is a single-phase material.

Figures 4(a) and 4(b) show the SEM pictures of a 0.4-μm $ErBa_2Cu_3O_{7-\delta}$ thin film on $LaAlO_3(100)$ substrate (magnification, 500 and 10 K). This film was post annealed at 850 °C. The film shows a typical surface morphology of the $RBa_2Cu_3O_{7-\delta}$ thin films grown by the BaF_2 technique, if their thickness is greater than 0.2 μm.[10–13] By electron microscopy studies, several groups have reported that the needlelike grains in the form of a net near the surface region are *a* oriented whereas the material under the netlike structure has a *c*-oriented growth.[10,11] There are also some bright regions on the surface which might be second-phase particulates or dust particles.

In Fig. 5, the SEM picture of a 0.4-μm $Er_5Ba_7Cu_{12}O_y$ thin film on a $LaAlO_3(100)$ substrate is shown (annealing

temperature = 850 °C; SEM magnification, 10 K). For the same sample, the XRD pattern was shown in Fig. 2(a). As described in Sec. III A, the film has both *c*- and *a*-oriented growths. The picture at 10 K magnification in Fig. 5 shows a small amount of netlike structure. But there are two major differences between the surface morphologies of the 0.4-μm $Er_5Ba_7Cu_{12}O_y$ thin film on $LaAlO_3(100)$ and the 0.4-μm $ErBa_2Cu_3O_{7-\delta}$ thin film on $LaAlO_3(100)$ (30-min anneal at 850 °C): (1) the amount of *a*-oriented growth for the $Er_5Ba_7Cu_{12}O_y$ thin film is much less; and (2) the *a*-oriented grains of $Er_5Ba_7Cu_{12}O_y$ are rodlike (thicker in cross section), whereas the *a*-oriented grains of $ErBa_2Cu_3O_{7-\delta}$ are needlelike.

Figures 6(a) and 6(b) show the SEM pictures of a 0.4-μm $Er_5Ba_7Cu_{12}O_y$ thin film on a $LaAlO_3(100)$ substrate, which was annealed at 870 °C (magnification, 500 and 10 K). There are very few particulates on the surface and the film displays a smooth surface morphology. The pictures were taken in the backscattering mode of SEM and the brightness of SEM was reduced to enhance the contrast of surface topography. The SEM pictures of a similar 0.4-μm $Er_5Ba_7Cu_{12}O_y$ thin film on a $SrTiO_3(100)$ substrate at magnifications of 500 and 10 K are depicted in Figs. 7(a) and 7(b). This film was annealed twice (annealing temperatures, 850 and 870 °C). Again, the surface is found to be smooth, but there are few *a*-oriented grains near the surface.

C. Four-point dc-resistivity measurements under magnetic fields

The superconducting resistive transitions of a 0.24-μm epitaxial $Er_5Ba_7Cu_{12}O_y(001)$ thin film on a $LaAlO_3(100)$ substrate under 0–5-T magnetic fields are shown in Figs. 8(a) and 8(b) for a constant dc current of 0.1 and 1.0 mA, respectively (four-point resistivity measurements). The magnetic field was applied in a direction perpendicular to the *ab* plane i.e., H is perpendicular to the film surface. The $T_{c,\text{onset}}$ is at about 93 K and the superconducting transition in low magnetic fields is sharp. The XRD studies revealed that the film has *c* epitaxy (XRD pattern not shown). This film was post annealed at 885 °C.

First, while neglecting the temperature dependence of activation energy, U, the data were fitted with the Anderson-Kim model of thermally activated flux creep [Eq. 3(b)]. The plots of $\log_{10}(\rho)$ versus $1000/T$ for 0.1- and 1-mA constant currents are shown in Figs. 9(a) and 9(b). In the low resistivity region below T_c (above $1000/T_c$) the curves are almost linear. In that region, a linear least-squares fit was made to get the activation energy, U, as a function of magnetic field, H. Figures 10(a) and 10(b) show the plots of U [in normalized units, U/k_B (K)] versus H for 0.1- and 1.0-mA constant currents. To determine the magnetic-field dependence of activation energy, i.e., to determine the constants U_0 and γ in Eq. (4),

(a)

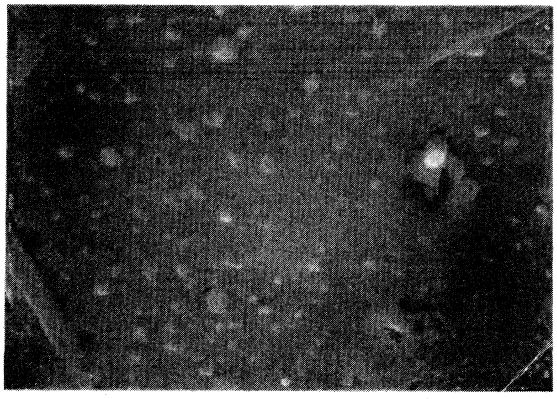

(b)

FIG. 3. SEM pictures of a 0.2-μm $Er_5Ba_7Cu_{12}O_y$ thin film on a $LaAlO_3(100)$ substrate (post-annealing temperature, $T_{\text{anneal}} = 890$ °C). The pictures were taken in the secondary electron detection mode of SEM. The surface is found to be smooth. The film is primarily *c* oriented, but there are few *a*-oriented grains which have a rod-like shape. (a) SEM magnification of 3 K, (b) SEM magnification of 10 K.

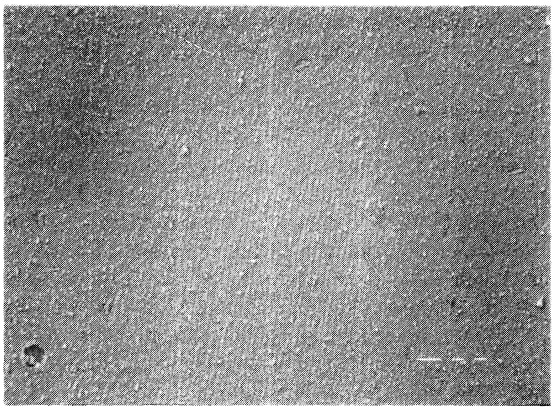

(a)

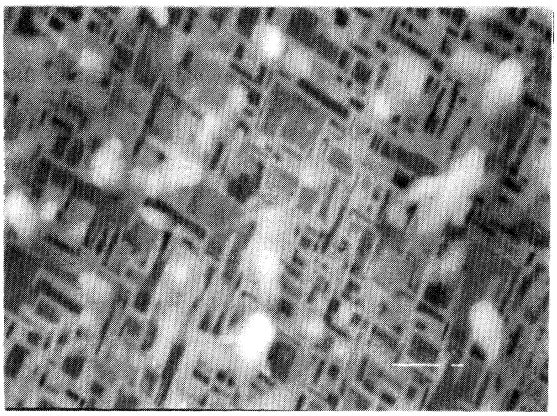

(b)

FIG. 4. SEM pictures of a 0.4-μm $ErBa_2Cu_3O_{7-\delta}$ thin film on a $LaAlO_3(100)$ substrate ($T_{anneal}=850$ °C). The pictures were taken in the backscattering mode of SEM. The netlike structure near the surface is formed by a-oriented grains of $ErBa_2Cu_3O_{7-\delta}$, as explained by several groups for this kind of surface morphology of the $RBa_2Cu_3O_{7-\delta}$ thin films with thicknesses ≥ 0.2 μm (Refs. 10 and 11). The region under the netlike structure is thought to be a c-oriented epilayer (Refs. 10 and 11). (a) SEM magnification of 500, (b) SEM magnification of 10 K.

the plots of $\log_{10}(U)$ versus $\log_{10}(H)$ were made as shown in Figs. 11(a) and 11(b) for 0.1- and 1.0-mA constant currents. Linear least-squares fits to the data yielded the constants U_0 (intercept on the y axis) and γ (slope). The values of U_0 [K T^{γ}] are 6607 and 5705 for 0.1- and 1-mA currents, and their respective values of γ are 0.39 and 0.36. Hence, the average U_0 is 6156 (or 6×10^3) K T^{γ} and $\gamma=0.375$.

The transport data were also analyzed with the giant flux-creep model. In this analysis, the temperature dependence as well as the magnetic-field dependence of activation energy U were taken into consideration [Eq. (5)]. Substitution of Eq. (5) in Eq. (3b) gives an equation for the resistivity. Using a value of 1.8 for α in Eq. (5), $\log_{10}(\rho/H)$ versus $[1000(1-t)^{\alpha}]/T$ were calculated ($t=T/T_c$, $T_c=92.5$ K). Figures 12(a) and 12(b) show the plots of $\log_{10}(\rho/H)$ versus $[1000(1-t)^{\alpha}]/T$ for 0.1 and 1.0-mA constant currents. The slopes of curves in the linear region below T_c on the right-hand side yielded a function of U_0 [see Eqs. (3b) and (5)], which can be described as

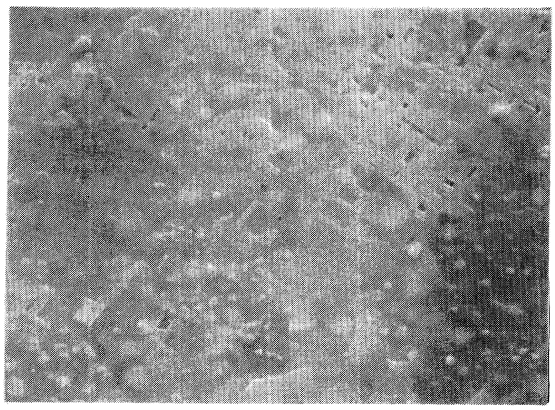

FIG. 5. SEM pictures of a 0.4-μm $Er_5Ba_7Cu_{12}O_y$ thin film on a $LaAlO_3(100)$ substrate ($T_{anneal}=850$ °C) at a magnification of 10 K. The film has c- and a-oriented grains as revealed by its XRD pattern in Fig. 1(a). The SEM was operated in the secondary electron detection mode. The thick rods of a-oriented grains are in a netlike structure near the surface. The amount of a-oriented grains of $Er_5Ba_7Cu_{12}O_y$ is much smaller than the amount of a-oriented grains of $ErBa_2Cu_3O_{7-\delta}$ in Fig. 4(b) for similar film thicknesses and post-annealing conditions.

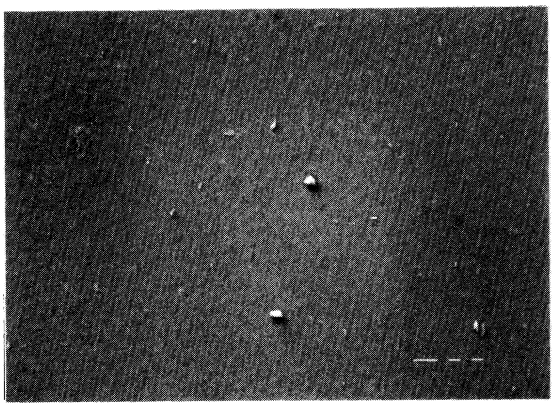

(a)

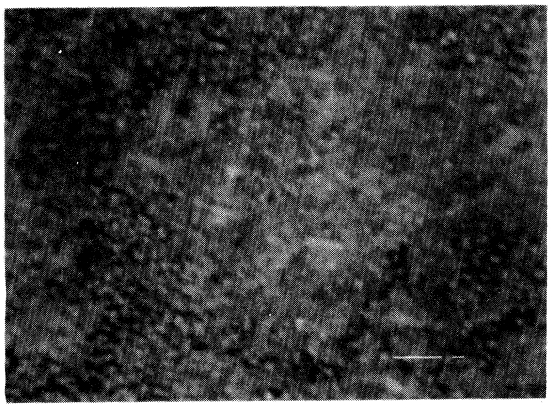

(b)

FIG. 6. SEM pictures of a 0.4-μm $Er_5Ba_7Cu_{12}O_y$ thin film on a $LaAlO_3$(100) substrate. The film was post-annealed twice ($T_{anneal}=850$ and 870 °C). The SEM pictures were taken in the backscattering mode of SEM. The brightness of the CRT screen of SEM was reduced to enhance the contrast of surface topography. The film shows a smooth surface and (001) epitaxy. The orientation of film growth was confirmed by XRD. (a) SEM magnification of 500, (b) SEM magnification of 10 K.

$F(U_0)=U_0/H^{\beta}$ (H perpendicular to ab plane), (7)

where the units of U_0 are K T^{β}. The plots of $F(U_0)$ versus $1/H$ were found to be nonlinear, which indicated that $\beta\neq 1$. Therefore, $\log_{10}[F(U_0)]$ versus $\log_{10}(1/H)$ were obtained as shown in Figs. 13(a) and 13(b) for 0.1- and 1.0-mA constant currents. The y-axis intercepts of linear least-squares fits to these plots gave the U_0 values of 34 041 and 27 227 [K T^{β} unit] for 0.1- and 1.0-mA constant currents, respectively. Neglecting the current dependence of activation energy in the regime of $J \ll J_c$. The average value of U_0 was computed as 30 634 (or 3×10^4) K T^{β}. The slopes of the linear least-squares fits in Figs. 13(a) and 13(b) were found to be 0.748 and 0.665. Hence, the average value of β is 0.7.

The data were also analyzed with $\alpha=1.5$. The results obtained with $\alpha=1.5$ were similar. Further data analysis and modeling will be carried out when extensive transport data are acquired in further experiments.

IV. DISCUSSION

A. Crystal structure

Our XRD results for the $Er_5Ba_7Cu_{12}O_y$ thin films indicated that the unit cell of $Er_5Ba_7Cu_{12}O_y$ is orthorhombic (Sec. III A). The lattice constants were determined to be $a_0=10.38$ Å, $b_0=10.52$ Å, $c_0=11.65$ Å, and $\alpha=\beta=\gamma=90°$. In comparison, the lattice constants of the orthorhombic unit cell of $ErBa_2Cu_3O_{7-\delta}$ are the following: $a_0'=3.83$ Å, $b_0'=3.85$ Å and $c_0'=11.65$ Å.[2] Hence, one of the lattice constants of $Er_5Ba_7Cu_{12}O_y$ and $ErBa_2Cu_3O_{7-\delta}$ is the same ($c_0=c_0'=11.65$ Å). To understand the relationships of the lattice constants of $Er_5Ba_7Cu_{12}O_y$ and $ErBa_2Cu_3O_{7-\delta}$ in the ab plane, a model can be used. Figure 14 depicts four unit cells of $ErBa_2Cu_3O_{7-\delta}$ in the ab plane (solid lines). The lattice constants a_0 and b_0 of $Er_5Ba_7Cu_{12}O_y$ are slightly smaller than AC and AE (dashed lines).

As mentioned earlier, the composition of $Er_5Ba_7Cu_{12}O_y$ is equivalent to the composition of four $ErBa_2Cu_3O_{7-\delta}$ with one excess Er atom and one less Ba atom. The results indicate that $Er_5Ba_7Cu_{12}O_y$ is not $Er_{1+x}Ba_{2-x}Cu_3O_y$ ($x=0.25$) structurally, i.e., there is no random substitution of Ba atoms by the excess Er atoms. In other words, a defect structure in each set of four unit cells of $ErBa_2Cu_3O_{7-\delta}$ with an excess Er atom and less Ba atoms is ordered so that the new unit cells of $Er_5Ba_7Cu_{12}O_y$ are formed. At this point, it is not very clear if the crystal structure of $Er_5Ba_7Cu_{12}O_y$ will be stable in the bulk processing conditions. In a thin-film

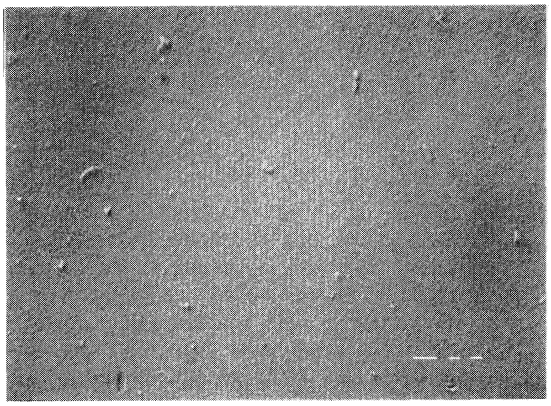

(a)

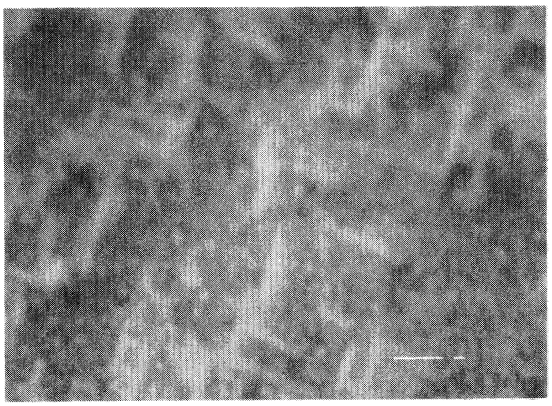

(b)

FIG. 7. SEM pictures of a 0.4-μm $Er_5Ba_7Cu_{12}O_y$ thin film on a $SrTiO_3(100)$ substrate. The film was annealed twice ($T_{anneal}=850$ and 870 °C). The SEM pictures were taken in the backscattering mode of SEM. The brightness of the CRT screen of SEM was reduced to enhance the contrast of surface topography. The film shows a smooth surface and *c* epitaxy. Few *a*-oriented grains are also observed. The XRD pattern of this film after the first anneal (850 °C) was shown in Fig. 1(b). (a) SEM magnification of 500, (b) SEM magnification of 10 K.

form, metastable crystal structures are found to be stable, which cannot be synthesized by the bulk processing techniques. For example, α Sn in the cubic (diamond) structure can be formed as epitaxial thin films but a solidified tin from its melt at temperatures above 13 °C is β Sn, which has a tetragonal structure, or γ Sn above 161 °C. One reason for the stability of thin-film metastable crystal structures is that in the case of thin films the surface energy and strain energy in epitaxial or oriented film growth make significant contributions to the total free energy, which determines the growth thermodynamics and phase stability.[24] The MBE technique of thin-film growth allows synthesis of metastable phases of materials which might not be displayed in the equilibrium phase diagrams.[24,25] Usually, the equilibrium phase diagram of a multicomponent system describes the phase relations and stability of compounds at a pressure of 1 atm. At this point, it should not be assumed that $Er_5Ba_7Cu_{12}O_y$ is not stable as a bulk material. In Sec. III A, we have seen that the 1.2-μm $Er_5Ba_7Cu_{12}O_y$ thin film on the cubic $ZrO_2(100)$ substrate gives a polycrystalline-type material [Fig. 2(a)]. Although the film is not thick enough to be a bulk material, the possibility of the existence of bulk $Er_5Ba_7Cu_{12}O_y$ is not ruled out.

B. Microstructure and surface morphology

The SEM pictures provided information on the microstructure of the oriented $Er_5Ba_7Cu_{12}O_y$ thin films. As shown in Sec. III B, a large amount of second phases was not observed. The SEM results on the microstructure of $Er_5Ba_7Cu_{12}O_y$ thin films support our earlier claim that the $Er_5Ba_7Cu_{12}O_y$ thin film is a single-phase material.

The surface morphology of the $Er_5Ba_7Cu_{12}O_y$ thin films was found to be very interesting. For 0.4-μm $Er_5Ba_7Cu_{12}O_y$ thin films on the $LaAlO_3(100)$ substrate, which are prepared by molecular-beam deposition and post annealing at 850 °C, the growth is dominated by (001) epitaxy, although there are few *a*-oriented grains in the surface region. For 0.4-μm $Er_5Ba_7Cu_{12}O_y$ thin films on $LaAlO_3(100)$ and $SrTiO_3(100)$ substrates post annealed in the 870–890 °C range, the films have a smooth surface morphology and *c*-oriented epitaxial growth. The smooth $Er_5Ba_7Cu_{12}O_y(001)$ thin films show a great potential for applications in high-T_c superconductor electronics because surface smoothness is desired for making superconductor microelectronic devices.

The shape of the *a*-oriented grains of $Er_5Ba_7Cu_{12}O_y$ thin films is also interesting. The *a*-oriented grains in the $Er_5Ba_7Cu_{12}O_y$ thin films are like thick rods. It suggests that the mechanical properties of $Er_5Ba_7Cu_{12}O_y$ and $ErBa_2Cu_3O_{7-\delta}$ thin films might not be the same.

C. Thermally activated flux-creep behavior

The transport data of superconducting resistive transitions under magnetic fields (0–5 T) were analyzed using

the models of thermally activated flux creep. In the Anderson-Kim model, the activation energy for flux creep for the $Er_5Ba_7Cu_{12}O_y(001)$ thin films is given by the expression

$$U(K)=6\times10^3H^{-0.375} \quad (H \text{ perpendicular to } ab \text{ plane}), \tag{8}$$

where H is T. In the giant flux-creep model for high-T_c superconductors, the experimentally derived T and H dependences of U for the $Er_5Ba_7Cu_{12}O_y(001)$ thin films can be described by the relationship

$$U(K)=[3\times10^4(1-t)^{1.8}]/H^{0.7} \quad (\text{H perpendicular to } ab \text{ plane}), \tag{9}$$

where the applied magnetic field is in T.

We would like to apply these two models to predict the activation energy at the liquid-nitrogen temperature (77 K) for 1-T magnetic field and H perpendicular to the ab plane. Using a value of 92.5 K for T_c, Eq. (8) gives a value of $U=6000$ K (0.52 eV) in the Anderson-Kim model whereas U is calculated to be 1200 K (0.1 eV) from Eq. (9) in the giant flux-creep model. In the first model, there is not temperature dependence of U. Hence, the first model is not useful for predicting the flux-creep behavior at low temperatures. The second model can be used to calculate the activation energy for flux creep at any temperature. For example, at $T=50$ K and $H=1$ T, Eq. (9) gives a U value of 7400 K (0.64 eV).

Obviously, the giant flux-creep model is more acceptable. However, as shown in a recent paper, in the case of pure $ErBa_2Cu_3O_{7-\delta}$ single crystals there is a vortex glass transition at about 74 K (T_g).[20] In the vortex glass transi-

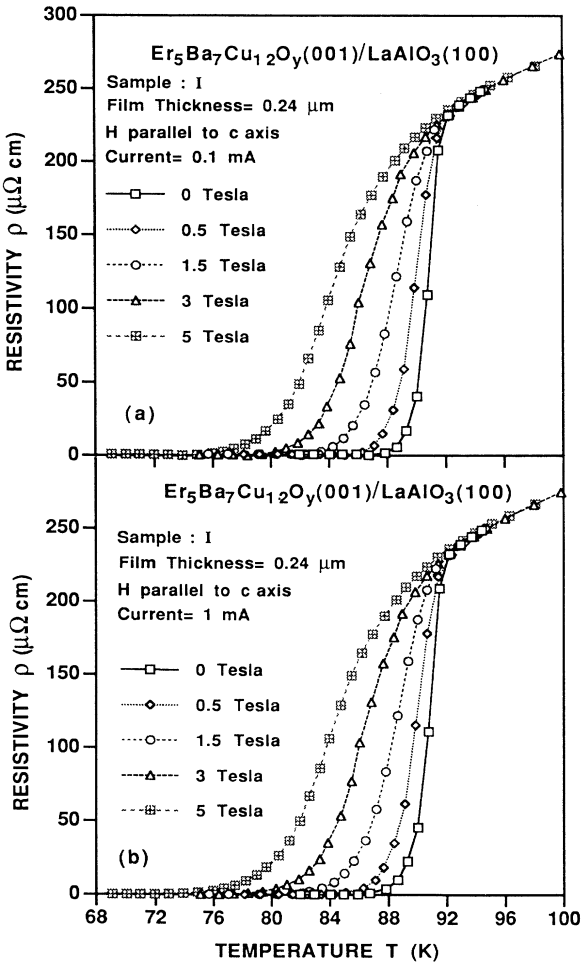

FIG. 8. Superconducting resistive transitions of a 0.24-μm epitaxial $Er_5Ba_7Cu_{12}O_y(001)$ thin film on a $LaAlO_3(100)$ substrate ($T_{anneal}=885$ °C) under 0–5 T magnetic fields. (a) ρ ($\mu\Omega$ cm) versus T (K) curves for an applied constant current of 0.1 mA in the four-point dc-resistivity measurements; (b) ρ ($\mu\Omega$ cm) versus T (K) curves for an applied constant current of 1 mA.

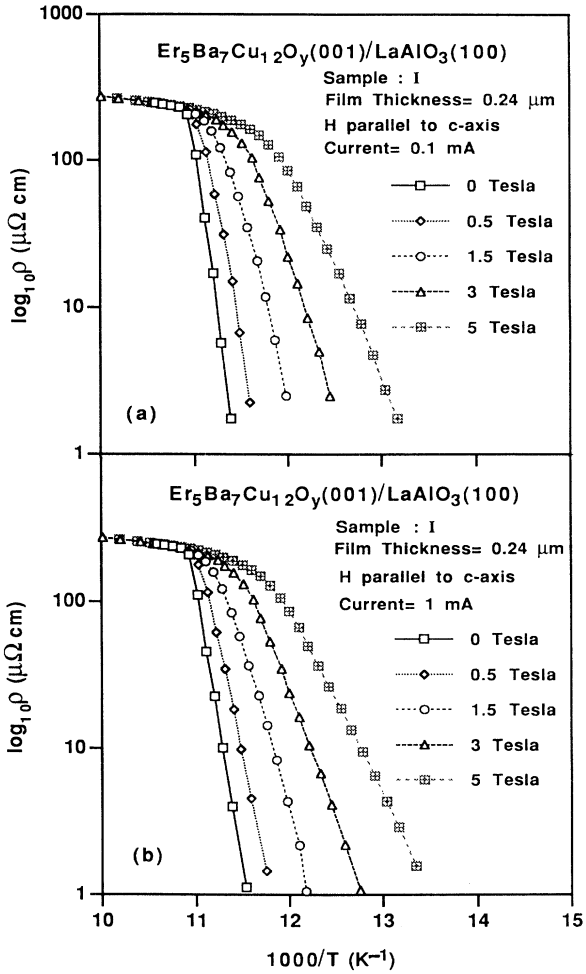

FIG. 9. $\log_{10}\rho$ ($\mu\Omega\,cm$) versus $1000/T$ (K^{-1}) curves for the data shown in Figs. 8(a) and 8(b) for the epitaxial 0.24-μm $ER_5Ba_7Cu_{12}O_y(001)$ thin film on a $LaAlO_3(100)$ substrate. (a) $\log_{10}\rho$ ($\mu\Omega$ cm) versus $1000/T$ (k^{-1}) for 0.1-mA constant current; (b) $\log_{10}\rho$ ($\mu\Omega$ cm) versus $1000/T$ (K^{-1}) for 1-mA constant current.

tion model, the resistance truly goes to zero.[21] Therefore, if the $Er_5Ba_7Cu_{12}O_y$ thin films also have a vortex glass transition near 74 K or at a lower temperature then it might not be necessary to predict flux creep at lower temperatures.

Sun *et al.* have studied the flux-creep behavior of *c*-oriented $ErBa_2Cu_3O_{7-\delta}$ thin films.[18] In the giant flux-creep model, their experimentally derived expression for the activation energy is given as

$$U = 27(\text{eV kG})(1-t)^{1.5}/H \quad (H \text{ perpendicular to } ab \text{ plane}), \quad (10)$$

where H is in kG (1 T = 10 kG). This equation predicts that at 1 T and 77 K the value of U for the $ErBa_2Cu_3O_{7-\delta}$ thin films is 0.15 eV. This compared well with our experimentally derived value of activation energy (0.1 eV) for the *c*-oriented $Er_5Ba_7Cu_{12}O_y$ thin films (H perpendicular to the *ab* plane $H = 1$ T and $T = 77$ K).

Hence, the results indicate that the flux-creep behavior of *c*-oriented $Er_5Ba_7Cu_{12}O_y$ and $ErBa_2Cu_3O_{7-\delta}$ thin films are similar. The value of the activation energy for flux creep also gives qualitative information on the strength of flux pinning and flux-pinning mechanisms. Since the flux pinning in $ErBa_2Cu_3O_{7-\delta}$ thin films is known to be strong, the $Er_5Ba_7Cu_{12}O_y$ thin films are expected to have a strong flux pinning. The mechanisms of flux pinning in $Er_5Ba_7Cu_{12}O_y$ and $ErBa_2Cu_3O_{7-\delta}$ thin films might also be similar. In $YBa_2Cu_3O_{7-\delta}$ single crystals, pinning by

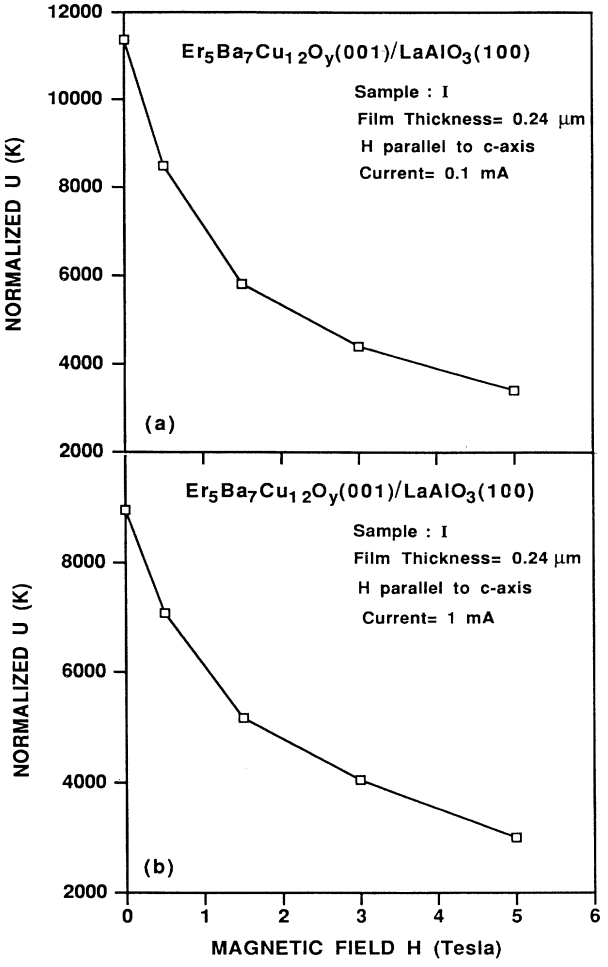

FIG. 10. Activation energy for flux creep, U, as a function of magnetic field (H perpendicular to the *ab* plane) for the 0.24-μm $Er_5Ba_7Cu_{12}O_y$(001) thin film on a $LaAlO_3$(100) substrate. The activation energy values were obtained from the slopes of linear least-squares fits to the data in the linear low-resistivity region of $\log_{10}\rho$ ($\mu\Omega$ cm) versus $1000/T$ (K^{-1}) curves [data points on the right-hand side in Figs. 9(a) and 9(b)]. The temperature dependence of U was neglected in this analysis. (a) U (in normalized units K) versus H (T) for 0.1-mA constant current; U (K) versus H (T) for 1-mA constant current.

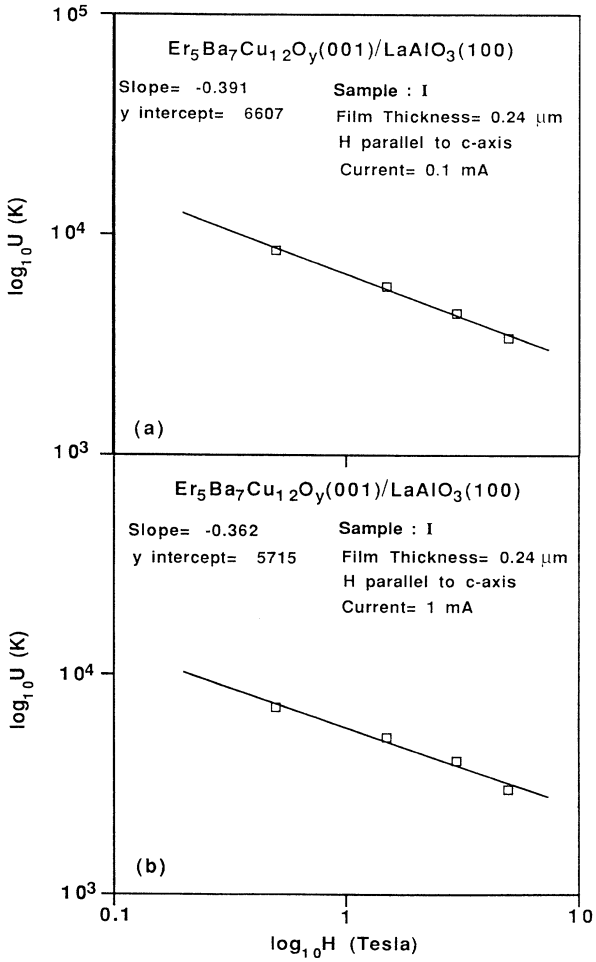

FIG. 11. Log-log plots of U (K) versus H corresponding to the data shown in Figs. 10(a) and 10(b) for the 0.24-μm $Er_5Ba_7Cu_{12}O_y$(001) thin film on a $LaAlO_3$(100) substrate. Linear least-squares fits were made to the data to obtain the constant U_0 and exponent γ according to Eq. (4) to describe the magnetic-field dependence of activation energy, U, for H perpendicular to the *ab* plane. (a) $\log_{10}U$ (K) versus $\log_{10}H$ (T) for 0.1-mA constant current; (b) $\log_{10}U$ (K) versus H (T) for 1-mA constant current.

grain boundaries as well as intrinsic pinning have been observed.[26]

In the analysis of transport data with the models of thermally activated flux creep, the tail region of the superconducting resistive transition curves have been used. In our experience, the tail region is also sensitive to the quality of samples. For the $ErBa_2Cu_3O_{7-\delta}$ and $Er_5Ba_7Cu_{12}O_y$ thin films grown by the BaF_2 technique, if the sample is not annealed for sufficient time then either the tail region expands significantly or the T_c drops. In those cases, the presence of a $Er_2Ba_4Cu_8O_y$-like material has been found by XRD, since a d spacing of about 27 Å is measured which corresponds to the lattice constant c_0 of $ErBa_2Cu_4O_8$ (Er248). It is well known that the Er248 phase is stable when the samples are post annealed at temperatures less than about 830 °C. In the post-annealing treatment when the samples are heated in wet O_2, the sample goes through the lower temperature range in which the formation of the Er248-like phase is favored, before it reaches the final annealing temperature (≥ 850 °C). In our resistivity measurements, it has been observed that the $ErBa_2Cu_3O_{7-\delta}$ or $Er_5Ba_7Cu_{12}O_y$ thin films mixed with a significant amount of the $Er_2Ba_4Cu_8O_y$-like material possess much lower resistivity, but the samples have a broad tail or lower T_c. When the thin films are annealed at ≥ 850 °C for sufficient time, the $Er_2Ba_4Cu_8O_y$-like phase reacts with other phases to form a single-phase $ErBa_2Cu_3O_{7-\delta}$ or $Er_5Ba_7Cu_{12}O_y$ thin film. Furthermore, the tail of a superconducting resistive

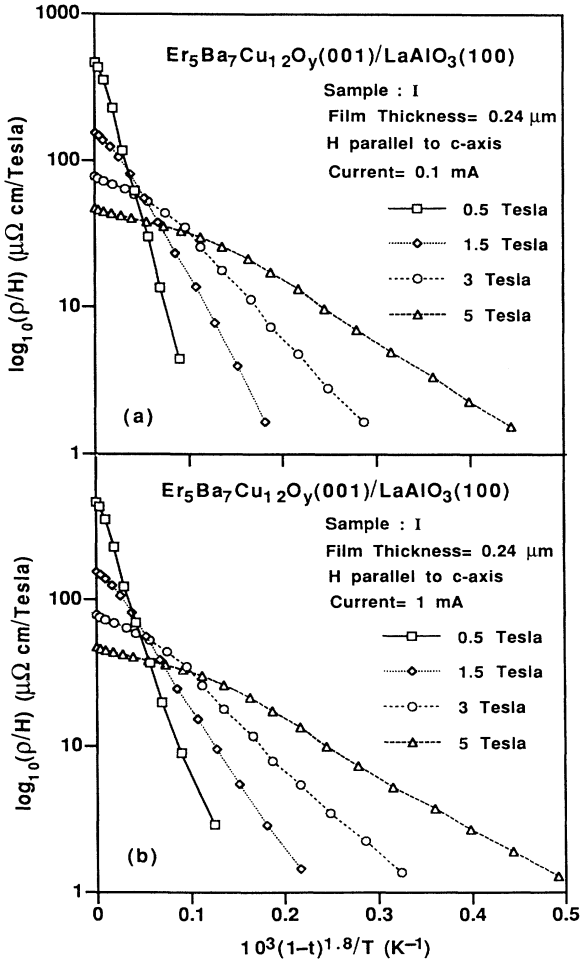

FIG. 12. $\log_{10}\rho/H$ ($\mu\Omega$ cm/T) versus $[1000(1-t)^{1.8}]/T$ (K^{-1}) curves for the data shown in Figs. 8(a) and 8(b) for the epitaxial 0.24-μm $Er_5Ba_7Cu_{12}O_y$(001) thin film on a $LaAlO_3$(100) substrate. These curves were used to calculate the activation energy for flux creep from Eqs. (3b) and (5). (a) $\log_{10}\rho/H$ ($\mu\Omega$ cm/T) versus $[1000(1-t)^{1.8}]/T$ (K^{-1}) for 0.1-mA constant current; (b) $\log_{10}\rho/H$ ($\mu\Omega$ cm/T) versus $[1000(1-t)^{1.8}]/T$ (K^{-1}) for 1-mA constant current.

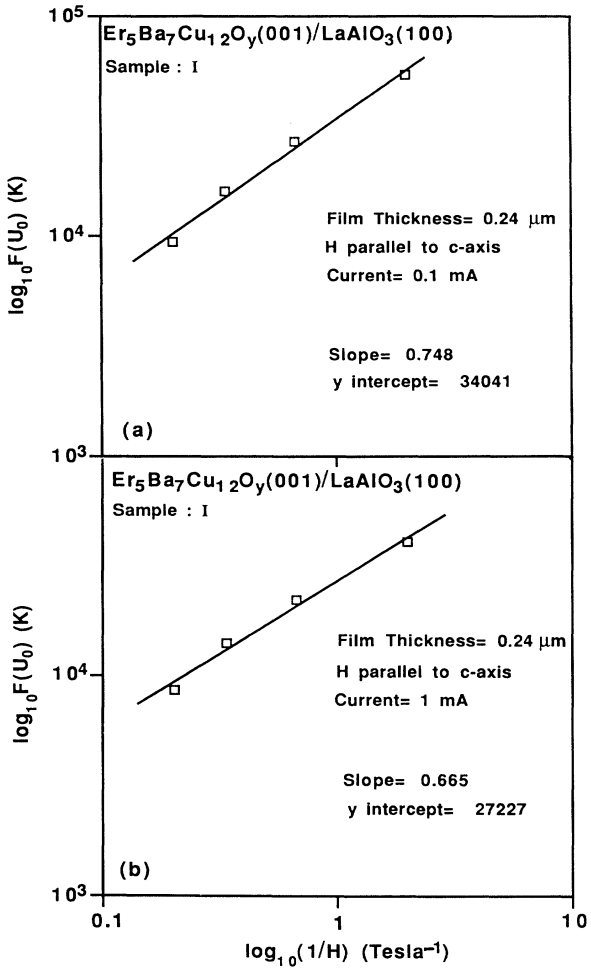

FIG. 13. Plots of function $F(U_0)$ versus $1/H$ on a log-log scale for the epitaxial 0.24-μm $Er_5Ba_7Cu_{12}O_y$(001) thin film on a $LaAlO_3$(100) substrate. The function $F(U_0)$ was obtained from the slopes of linear least-squares fits to the data in the linear low resistivity region of $\log_{10}\rho/H$ versus $[1000(1-t)^{1.8}]/T$ curves [data points on the right-hand side in Figs. 12(a) and 12(b)]. (a) $F(U_0)$ (K) versus H (T) for 0.1-mA constant current; (b) $F(U_0)$ (K) versus H (T) for 1-mA constant current. The y-axis intercepts and slopes of these log-log plots were calculated with linear least-squares fits to obtain the parameters U_0 with β according to Eq. (5).

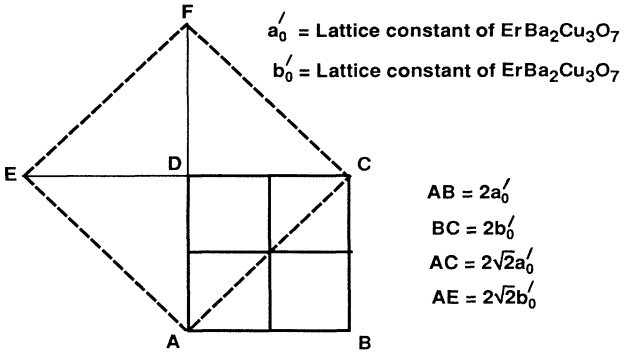

FIG. 14. A model of the relationships between the unit cells of $ErBa_2Cu_3O_{7-\delta}$ and $Er_5Ba_7Cu_{12}O_y$ in the *ab* plane. The figure shows four unit cells of $ErBa_2Cu_3O_{7-\delta}$ in the *ab* plane (solid lines). The lattice constants a_0 and b_0 of $Er_5Ba_7Cu_{12}O_y$ are slightly smaller than *AC* and *AE* (dashed lines).

transition curve becomes very big if the film composition is not controlled well during the molecular-beam deposition process. Therefore, the $Er_5Ba_7Cu_{12}O_y$ thin films for the flux-creep studies were always checks for their purity by XRD.

V. CONCLUSIONS

$Er_5Ba_7Cu_{12}O_y$ thin films on $LaAlO_3(100)$, $SrTiO_3(100)$, cubic $ZrO_2(100)$, and MgO(100) substrates grown by molecular-beam deposition and post annealing were studied by x-ray diffraction, scanning electron microscopy, and four-point dc-resistivity measurements under magnetic fields. Some of the $Er_5Ba_7Cu_{12}O_y$ thin films on $LaAlO_3(100)$ and $SrTiO_3(100)$ substrates annealed at 850 °C grew with mixed *c* and *a* orientations, but most of the films were *c* oriented. The $Er_5Ba_7Cu_{12}O_y$ films on cubic $ZrO_2(100)$ and MgO(100) substrates had mixed *b* and *c* orientations. By XRD, the lattice parameters of the $Er_5Ba_7Cu_{12}O_y$ thin film were determined to be $a_0=10.38$ Å, $b_0=10.52$ Å, $c_0=11.65$ Å, $\alpha=\beta=\gamma=90°$.

In the scanning electron microscopy studies, the *c*-oriented $Er_5Ba_7Cu_{12}O_y$ thin films on $LaAlO_3(100)$ and $SrTiO_3(100)$ substrates were found to be smooth if (1) the post-annealing temperature was in the 870–880 °C range and (2) the film thickness was ≤ 0.4 μm. Furthermore, the *a*-oriented grains of $Er_5Ba_7Cu_{12}O_y$ thin films were found to be thick-rod-like in shape.

By the dc-resistivity measurements under magnetic fields, the flux-creep behavior of epitaxial $Er_5Ba_7Cu_{12}O_y(001)$ thin films was studied. For the $Er_5Ba_7Cu_{12}O_y$ thin films under magnetic fields (0–5 T), the experimentally derived values of activation energy for flux creep can be described by the relationship $U(K)=[3\times10^4(1-t)^{1.8}]/H^{0.7}$ (H perpendicular to the *ab* plane). At $H=1$ T and $T=77$ K, the equation gives an activation energy value of 1200 K or 0.1 eV. The activation energy values for *c* oriented $Er_5Ba_7Cu_{12}O_y$ and $ErBa_2Cu_3O_{7-\delta}$ thin films were found to be similar.

ACKNOWLEDGMENTS

This research was supported by the Midwest Superconductivity Consortium (MISCON), Purdue University, under Department of Energy Grant No. DE-FG02-90ER45427. We would like to thank Professor Mike McElfresh, Purdue University, Department of Physics, for allowing us to use his facilities for the transport measurements. We thank Professor Paul McGinn at the University of Notre Dame for helping us in the SEM experiments. We are grateful to Dr. Elliot Hartford, AT&T Bell Laboratory, for analyzing our samples by Rutherford backscattering spectroscopy. Finally, we thank the MISCON staff for their encouragement and support of superconductivity research. The RBS studies of *c*-oriented $Er_5Ba_7Cu_{12}O_y$ and $ErBa_2Cu_3O_{7-\delta}$ thin films on $LaAlO_3(100)$ substrates were performed by Dr. Elliot Hartford at AT&T Bell Laboratory, Murray Hill, New Jersey.

[1] *High-Temperature Superconductivity,* edited by J. W. Lynn (Springer-Verlag, New York, 1990).

[2] R. Beyer and T. M. Shaw, in *Solid State Physics,* edited by H. Ehrenreich and D. Turnbull (Academic, New York, 1989), Vol. 42.

[3] *High-Temperature Superconductivity: An Introduction,* edited by G. Burns (Academic, New York, 1991).

[4] *Physics of High-T_c Superconductors,* edited by J. C. Philips (Academic, New York, 1989).

[5] K. M. Choudhary, P. Seshadri, and J. Bae, Phys. Rev. B **45**, 4892 (1992).

[6] T. Iwata, M. Hitita, Y. Tajima, and S. Tsurumi, Jpn. J. Appl. Phys. **26**, L2049 (1987).

[7] K. M. Choudhary, J. Bae, P. Seshadri, and M. Sankararaman, J. Solid State Chem. **100**, 379 (1992); K. M. Choudhary, J. Bae, and P. Seshadri, *ibid.* **100**, 388 (1992).

[8] K. M. Choudhary, P. Seshadri, and J. Bae (unpublished).

[9] For the $Er_5Ba_7Cu_{12}O_y(001)/LaAlO_3(100)$ thin films, the Er to Ba ratio was confirmed to be 5:7. The samples might have 10% Cu deficiency. But the estimate of RBS signal from Cu is less accurate since the RBS signal from La from the $LaAlO_3$ substrate interfered with the Cu signal.

[10] A. Mogro-Campero, L. G. Turner, E. L. Hall, M. F. Garbauskas, and N. Lewis, Appl. Phys. Lett. **54**, 2719 (1989).

[11] M. P. Siegal, J. M. Phillips, Y.-F. Hsieh, and J. H. Marshall, Physica C **172**, 282 (1990).

[12] M. P. Siegal, J. M. Phillips, A. F. Hebard, R. B. van Dover, R. C. Farrow, T. H. Tiefel, and J. H. Marshall, J. App. Phys. **70**, 4982 (1991).

[13] P. M. Mankiewich, J. H. Scofield, W. J. Skocpol, R. E. Howard, A. H. Dayem, and E. Good, Appl. Phys. Lett. **51**, 1753 (1987).

[14] P. W. Anderson and Y. B. Kim, Rev. Mod. Phys. (to be published).

[15] Y. Yeshurun and A. P. Malozemoff, Phys. Rev. Lett. **60**, 2202 (1988).

[16] M. Tinkham, Phys. Rev. Lett. **61**, 1658 (1988).

[17] S. Zhu, D. K. Christen, C. E. Klabunde, J. R. Thompson, E.

C. Zones, R. Feenstra, D. H. Lowndes, and D. P. Norton, Phys. Rev. B **46**, 5576 (1992).

[18]J. Z. Sun, K. Char, M. R. Hahn, T. H. Geballe, and A. Kapitulnik, Appl. Phys. Lett. **54**, 663 (1989).

[19]T. T. M. Palstra, B. Batlogg, R. B. van Dover, L. F. Schneemeyer, and J. V. Waszczak, Phys. Rev. B **41**, 6621 (1990).

[20]H. Safar, Bull. Am. Phys. Soc. **38**, 635 (1993).

[21]M. P. A. Fisher, Phys. Rev. Lett. **62**, 1415 (1989); R. H. Koch, V. Foglietti, W. J. Gallagher, G. Koren, A. Gupta, and M. P. A. Fisher, *ibid.* **63**, 1511 (1989).

[22]*Electron Microscopy of Materials: An Introduction,* edited by M. Von Heimendahl (Academic, New York, 1980).

[23]R. Jenkins, in *Advances in X-Ray Anaysis,* edited by C. R. Hubbard *et al.* (Plenum, New York, 1982), Vol. 26, p. 25.

[24]*Materials Fundamentals of Molecular Beam Epitaxy,* edited by J. Y. Tsao (Academic, New York, 1993).

[25]R. L. Gunshor, L. A. Kolodziejski, A. V. Nurmikko, and N. Otsuka, in *Strained-Layer Superlattices: Materials Science and Technology,* edited by T. P. Pearsall (Academic, Boston, 1991), Vol. 33.

[26]G. J. Dolan, G. V. Chandrashekhar, T. R. Dinger, C. Feidl, and F. Holtzberg, Phys. Rev. Lett. **62**, 827 (1989).

Film: $Er_5Ba_7Cu_{12}O_y$
Substrate: $LaAlO_3$
Thickness: 0.2 μm
T_{anneal}: 890 °C
Sample : E

Magnification: 3000

(a)

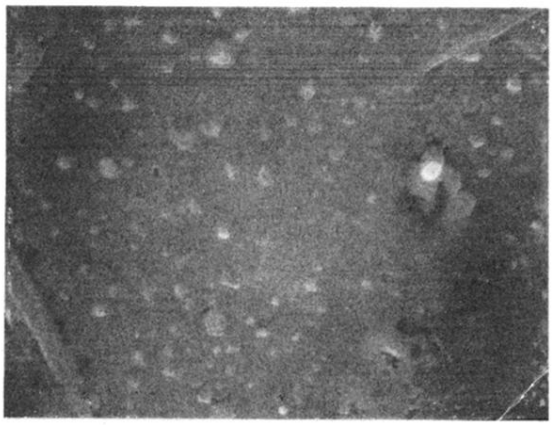

Film: $Er_5Ba_7Cu_{12}O_y$
Substrate: $LaAlO_3$
Thickness: 0.2 μm
T_{anneal}: 890 °C
Sample : E

Magnification: 10000

(b)

FIG. 3. SEM pictures of a 0.2-μm $Er_5Ba_7Cu_{12}O_y$ thin film on a $LaAlO_3$(100) substrate (post-annealing temperature, T_{anneal} = 890 °C). The pictures were taken in the secondary electron detection mode of SEM. The surface is found to be smooth. The film is primarily c oriented, but there are few a-oriented grains which have a rod-like shape. (a) SEM magnification of 3 K, (b) SEM magnification of 10 K.

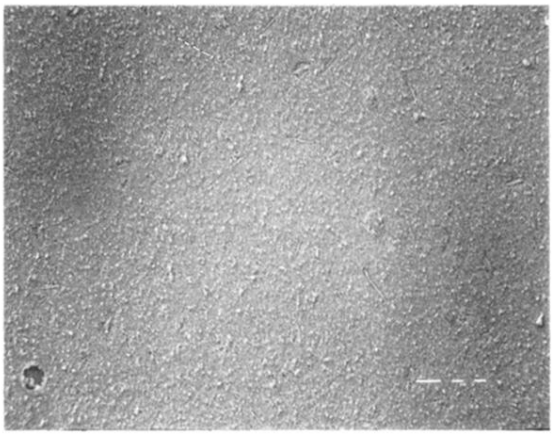

(a)

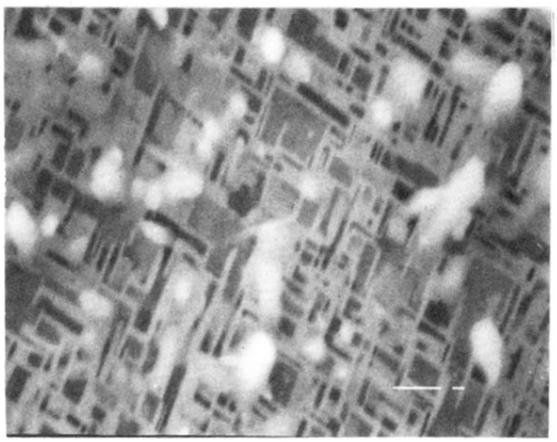

(b)

FIG. 4. SEM pictures of a 0.4-μm $ErBa_2Cu_3O_{7-\delta}$ thin film on a $LaAlO_3$(100) substrate ($T_{anneal}=850\,^{\circ}C$). The pictures were taken in the backscattering mode of SEM. The netlike structure near the surface is formed by a-oriented grains of $ErBa_2Cu_3O_{7-\delta}$, as explained by several groups for this kind of surface morphology of the $RBa_2Cu_3O_{7-\delta}$ thin films with thicknesses ≥ 0.2 μm (Refs. 10 and 11). The region under the netlike structure is thought to be a c-oriented epilayer (Refs. 10 and 11). (a) SEM magnification of 500, (b) SEM magnification of 10 K.

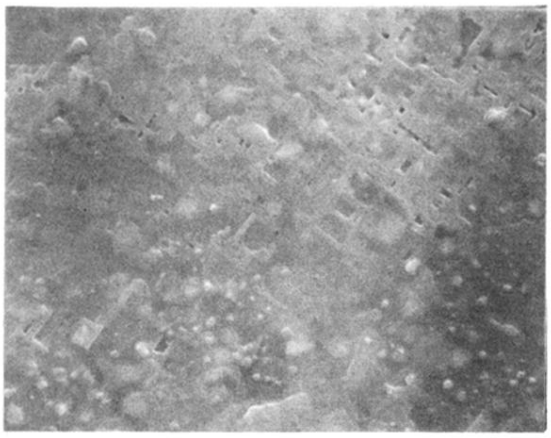

FIG. 5. SEM pictures of a 0.4-μm $Er_5Ba_7Cu_{12}O_y$ thin film on a $LaAlO_3$(100) substrate ($T_{anneal}=850$ °C) at a magnification of 10 K. The film has *c*- and *a*-oriented grains as revealed by its XRD pattern in Fig. 1(a). The SEM was operated in the secondary electron detection mode. The thick rods of *a*-oriented grains are in a netlike structure near the surface. The amount of *a*-oriented grains of $Er_5Ba_7Cu_{12}O_y$ is much smaller than the amount of *a*-oriented grains of $ErBa_2Cu_3O_{7-\delta}$ in Fig. 4(b) for similar film thicknesses and post-annealing conditions.

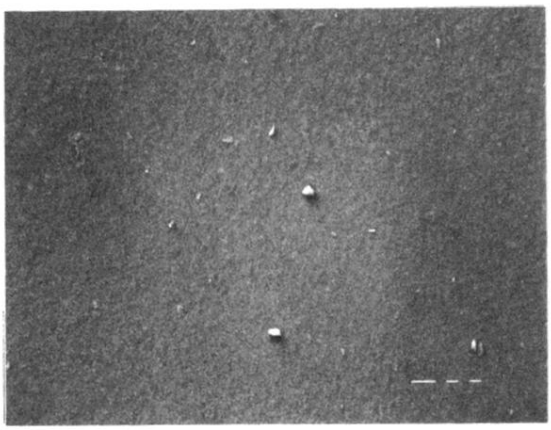

(a)

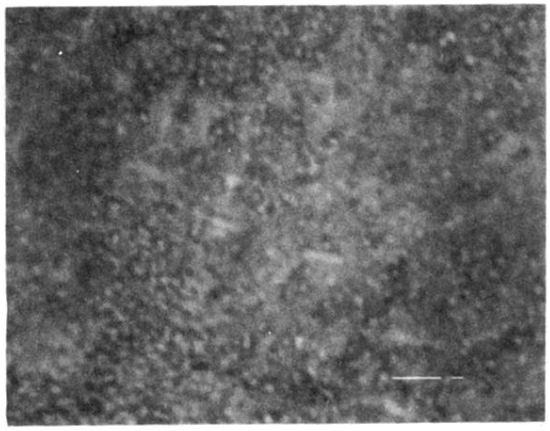

(b)

FIG. 6. SEM pictures of a 0.4-μm $Er_5Ba_7Cu_{12}O_y$ thin film on a $LaAlO_3$(100) substrate. The film was post-annealed twice (T_{anneal} = 850 and 870 °C). The SEM pictures were taken in the backscattering mode of SEM. The brightness of the CRT screen of SEM was reduced to enhance the contrast of surface topography. The film shows a smooth surface and (001) epitaxy. The orientation of film growth was confirmed by XRD. (a) SEM magnification of 500, (b) SEM magnification of 10 K.

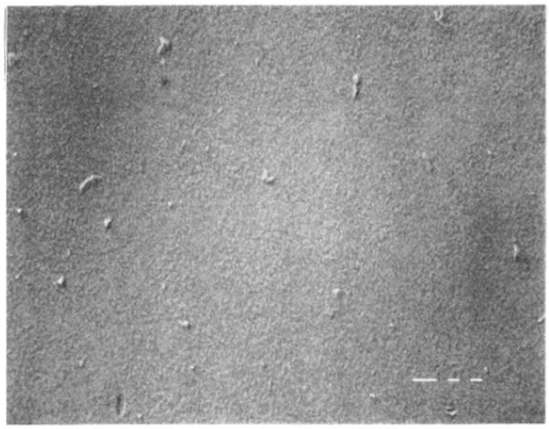

(a)

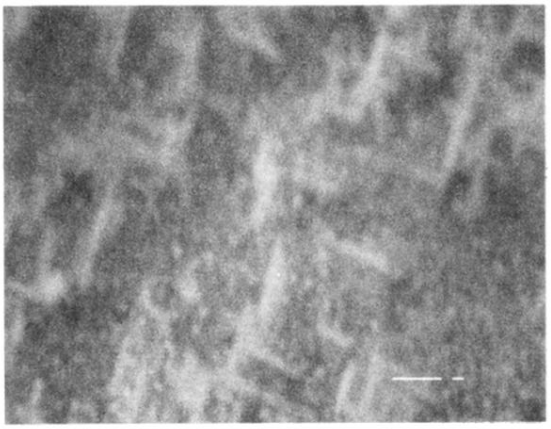

(b)

FIG. 7. SEM pictures of a 0.4-μm $Er_5Ba_7Cu_{12}O_y$ thin film on a $SrTiO_3$(100) substrate. The film was annealed twice (T_{anneal} = 850 and 870 °C). The SEM pictures were taken in the backscattering mode of SEM. The brightness of the CRT screen of SEM was reduced to enhance the contrast of surface topography. The film shows a smooth surface and *c* epitaxy. Few *a*-oriented grains are also observed. The XRD pattern of this film after the first anneal (850 °C) was shown in Fig. 1(b). (a) SEM magnification of 500, (b) SEM magnification of 10 K.